https://doi.org/10.37434/tpwj2021.09.05

MODELING OF THE PROCESS OF INDUCTION HEAT TREATMENT OF WELDED JOINTS FROM RAIL HIGH-STRENGTH STEELS

R.S. Hubatyuk, S.V. Rymar, O.S. Prokofiev, V.A. Kostin, O.V. Didkovskyi and **E.V. Antipin**
E.O. Paton Electric Welding Institute of the NAS of Ukraine
11 Kazymyr Malevych Str., 03150, Kyiv, Ukraine. E-mail: office@paton.kiev.ua

The selection of technological parameters of the heat treatment process, which provides the necessary structural and phase transformations of rail welded joint, is a very expensive process that requires a large number of experiments with a significant consumption of power, time, labor and financial resources. The paper proposes the method of mathematical and physical modeling of thermal processes to determine the optimal parameters of heat treatment of rail welded joint on model specimens based on the theory of similarity, taking into account the interrelated properties and physical phenomena with the original study. The solutions obtained during realization of this method provide a considerable reduction of resources at determination of optimum modes of heating of products from high-strength carbon steels, in particular, rails. Based on the scale factors of criteria of electromagnetic and thermal similarity, a mathematical model of the induction system for numerical calculation of propagation of electromagnetic and thermal fields was developed. The finite element method was used, which represents a tool for combining integral characteristics with the values of vector characteristics of the studied electromagnetic fields. The dependence of physical properties of materials on temperature was taken into account. In the course of parametric study, the parameters and configuration of the «inductor–product» system were determined and the space-time distribution of the temperature field during heat treatment modeling was determined. The obtained data of numerical calculation should be used during physical modeling of optimization of the modes of heat treatment of the sample and will significantly reduce the number of experiments to determine the effect of thermal heating on phase transformations and mechanical properties of steel in the zone of welded joint. 18 Ref., 2 Tables, 9 Figures.

Keywords: induction heating, heat treatment, welded joint of railway rails, mathematical modeling, similarity theory

At present, laying of continuous tracks is performed at construction and reconstruction of the main railways. This is due to the general tendency of increase of rolling stock speed, particularly for high-speed passenger trains, increased traffic intensity and traffic density. In order to ensure a higher reliability and operational durability of the rails, new generation high-strength rail steels with higher carbon content are used, when laying the continuous tracks [1].

At construction of the railway tracks, high-strength rails are joined by welding their end faces. The joints are mostly made by flash-butt welding process developed at PWI [2], or automatic electric arc fusion welding. World experience shows that in the removed defective rails the weld is the region, where up to 30 % of defects are observed. Although defects in the weld are not predominant, they deserve close attention at control of the rail track quality. Inhomogeneity of the metal microstructure is found in the welded joint zone, and unfavourable residual stresses are observed, which create the conditions for formation of internal defects, weakening the rail section with the weld. The HAZ of the rail welded joint has different sections, characterized by the presence of soft metal layers on the rail rolling surface and layer of lower ductility and toughness, more prone to brittle fracture, compared to the rail base metal.

Higher carbon content cardinally changes the steel weldability. In terms of one of the main indices of steel weldability, namely carbon equivalent C_e, the rail steel is close to the high-strength medium-alloyed steels with 0.30–0.45 % carbon content. The values of carbon equivalent for these steels are approximately the same: C_e = 0.8–1.0 %. It points to the fact that by the weldability criterion the current high-strength rail steels belong to satisfactory ones, i.e. to those which require special welding modes and technological measures, without which it is impossible to ensure the integrity and quality of the welded joint [1].

One of such measures is heat treatment (HT) of the rail welded joint, which minimizes the consequences of the high-temperature heating of metal during weld-

R.S. Hubatyuk — https://orcid.org/0000-0002-0851-743X, S.V. Rymar — https://orcid.org/0000-0003-0490-4608,
O.S. Prokofiev — https://orcid.org/0000-0003-4643-6611, V.A. Kostin — https://orcid.org/0000-0002-2677-4667,
O.V. Didkovskyi — https://orcid.org/0000-0001-5268-5599, E.V. Antipin — https://orcid.org/0000-0003-3297-5382

ing, refines its microstructure, increases the welded joint strength, and relieves residual stresses. HT application has a positive impact on the service life of the rail butt joint [3].

Purpose and objectives of the study. The purpose and objectives of the study is development of a mathematical model for numerical modeling of the process of high-frequency induction heating of a model sample from high-carbon high-strength rail steel with a welded joint with determination of the parameters and configuration of «inductor–product» system for further performance of a real induction HT of a model sample, as well as determination of space-time distribution of the temperature field during HT performance.

Here, in order to shorten the time for calculation, it is rational to divide the mathematical modeling process into two stages: first — modeling of the process of high-frequency induction heating of «inductor–product» system; second — modeling of the structure of phase transformations and properties of the weld metal in the product, depending on the thermal cycle.

The following objectives were defined, in order reach the purpose:

- develop the concept of physical modeling of induction HT of welded joints of high-strength railway rails on model samples;
- using the physical model as a basis, develop a mathematical model for numerical calculation of induction heating of a model sample with the welded joint from high-strength rail steel;
- develop a mock-up and perform experimental studies on physical modeling of induction heating of a model sample.

Analysis of published data and problem definition. Analysis of application of computational models of induction heating systems shows wider application of numerical modeling methods when solving the problems of optimization of technological parameters of HT process. Numerical modeling of induction systems enabled studying not only individual aspects of electromagnetic and thermal field propagation, but also the accompanying phenomena and processes, such as stress-strain state and structural transformations of metal, and developing multiphysics models, taking into account the inextricable connection between these processes and physical phenomena.

In work [4] at development of a mathematical model of an induction heating system methods of induction system analysis are proposed, which enable consistently taking into account the nonlinear dependencies of thermophysical properties of the metal being heated, and in [5] the method of parametric optimization with distributed parameters was used. However, here the transformations in steel when exceeding the temperature of magnetic transformation points are ignored, that introduces an error at calculation of energy characteristics of the studied induction system.

In [6, 7] at development of a numerical model of induction heating of bodies of different cross-section with inhibition of the edge and end effects, a more uniform temperature field in the billet is achieved through application of the technological measures of changing the number of inductor sections, current frequency, different designs of magnetic concentrators, regulation of the speed of billet movement, etc. Here, the dependence of the billet magnetic permeability either on temperature, or on the magnetic field intensity is not taken into account.

Induction heating models from works [8, 9] use temperature-dependent *B*–*H* curves, nonlinear dependencies of the material thermophysical properties and change of phase transformation during sample heat treatment at rapid heating and cooling. Used as the model sample material is base metal of the studied object, homogeneous over the entire cross-section, which was not subjected either to thermal or to mechanical impact before that. Modeling is performed on samples in keeping with the normative standards or samples of an arbitrary shape and geometrical dimensions without indicating the criteria for selection of a particular parameter that influences the accuracy of the obtained results at transition from physical modeling on model samples to real objects and real technological process.

In view of the fact that the modern technologies of induction HT are not always optimal and do not allow fully obtaining the required characteristics of metal in the zone of rail welded joints [1], it becomes necessary to perform further investigations and study the features of phase transformations in the rail welded joint after HT. Performance of high-quality HT requires refining the modes and optimizing the parameters, influencing the heating processes, conducting a large scope of costly research on the effect of heating rates, soaking and cooling time on the features of structure formation in the welded joint zone. Solving this kind of problems requires an integrated approach that includes rational application of mathematical and physical modeling methods for investigations, and determination of key parameters of HT process. It is urgent and rational to solve such a problem first by modeling on small model samples of rail steel welded joints. For this purpose it is necessary to develop on the base of the theory of similarity the mathematical model of HT process of model samples, taking into account the interrelated properties and physical phe-

nomena with the studied original. A small model sample can be used to optimize the heating modes and to study the properties of the treated weld metal, which is followed by transition to refining the modes of HT of a butt welded joint of a real rail [10]. The proposed approach enables greatly reducing the resources used at determination of optimum modes of heating products from high-strength carbon steels, in particular, rails. Developed models of induction HT process will allow optimizing the inductor design to ensure the required temperature field in the zone of the welded joint of the object being heated, and it allows a more effective performance of HT process.

Methodology and methods of investigation of the induction system. At induction heating the electromagnetic and thermal processes are interrelated, and they are described by nonlinear differential equations, which cannot be solved analytically. This kind of problems can be solved only by numerical methods. The finite element method is extensively used for modeling the induction heating systems. This method is a tool for correlating the integral characteristics with the values of vector characteristics of the studied fields. The problem of induction heating modeling belongs to multiphysics problems that involve interrelated calculations of propagation of the electromagnetic and thermal fields [11].

At temperature variation in a broad range it is important to take into account also the change of physical properties of the materials, as it has a significant impact on the electromagnetic and thermal characteristics of «inductor-product» system. For correct solution by mathematical modeling of the process of induction HT, and in order to solve the interrelated problems of propagation of the electromagnetic and thermal fields it is rational to use multiphysics software packages of finite element analysis, for instance Comsol Multiphysics.

The object of study is «inductor–product» induction system, which consists of a cylindrical multiturn inductor that covers a cylindrical sample in the form of a solid rod from high-strength rail steel with increased carbon equivalent that has a transverse welded joint.

Introduced simplifications. The complex shape of the rail cross-section and different weight and size parameters of the rail main parts do not allow performing mathematical modeling of the process of induction HT in the two-dimensional or axisymmetric definition of the problem, but only in 3D formulation that requires considerable computational resources and quite considerable computer time. In order to obtain a faster evaluation result of mathematical and physical modeling of the process of induction heating

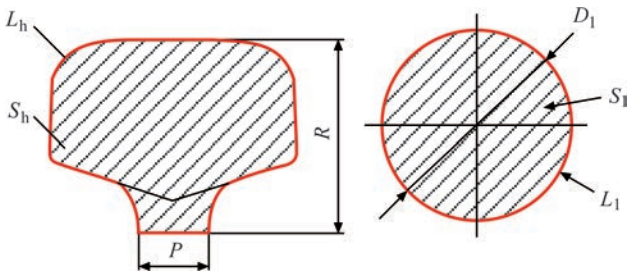

Figure 1. Transverse sections of the rail head and the solid cylindrical rod, which replaces it

of the rail butt welded joint, it was proposed to reduce the rail cross-section to a simpler form and to separately study induction heating of the main rail elements — head, web and foot. Here, these elements are replaced by simple figures: solid (for the head) and hollow (for the web and foot) cylindrical rods with equal parameters, surface areas and weights of the rail and rod elements. More over, in order to simplify physical modeling of the heating, these simple figures can be further reduced, by applying the similarity theory [12, 13].

As an example, let us consider the rail head, which is the most prone to dynamic loads, wear of the rolling surface and is susceptible to initiation of defects and cracks in the transverse weld zone. The head contains layers of hardened, transition and base metal.

The cross-section of the rail head in Figure 1 is presented in the form of a solid cylindrical rod of diameter D_1, perimeter L_1 and area S_1, which are equal to the perimeter of the heating zone under the inductor of head L_h and head area S_h. Such a geometrical transformation allows preserving the weight and size parameters of the head and the rod, and ensures correct results of physical modeling. In the site of the anticipated axial section P of the rail a condition is accepted that the temperature of this region is the same as that of the head surface and no heat removal occurs in this direction.

The criteria of geometrical, and electrodynamic similarity and similarity of thermal processes allow determination of the parameters of the mathematical and physical model, geometrical dimensions of a cylindrical sample with a transverse welded joint, and frequency of inductor supply current. The geometrical parameters of the inductor are determined when solving this problem.

To simplify further physical modeling of induction heating, we will reduce the overall dimensions of the cylindrical full-scale rod shown in Figure 1, to a model rod, introducing scale factors into consideration [13, 14].

Scale factors, similarity of electromagnetic processes. For induction system under consideration, we will assume the scales of magnetic induction m_B, mag-

netic permeability m_μ of steel, magnetic field intensity m_h and specific electric resistance m_ρ of full-scale 1 and model 2 rods to be equal to a unity that is valid in the case of using steel with the same electrophysical characteristics:

$$m_B = \frac{B_1}{B_2} = 1, \quad m_\mu = \frac{\mu}{\mu_2} = 1,$$
$$m_H = \frac{H_1}{H_2} = 1, \quad m_\rho = \frac{\rho_1}{\rho_2} = 1, \tag{1}$$

where B_1, B_2; μ_1, μ_2; H_1, H_2; ρ_1, ρ_2 are the magnetic induction, magnetic permeability, magnetic field intensity and specific electric resistance in the full-scale and modeled rods, respectively, which are accordingly equal to each other.

We will assume the following main linear l geometrical dimensions: diameters of full-scale and model cylindrical rods d_1, d_2; length of magnetic lines of force in the rods under the inductor l_1, l_2 (close to inductor length in the considered models); depth of penetration of magnetic fluxes and induced currents in the rod Δ_1, Δ_2. The scale of linear dimensions m_l, equal to the ratio of the mentioned geometrical dimensions, will be equal to:

$$m_l = \frac{d_1}{d_2} = \frac{\Delta_1}{\Delta_2} = \frac{l_1}{l_2}. \tag{2}$$

Depth of penetration of the induced currents in the full-scale and model rods for steel is [15]:

$$\Delta_{1,2} = \frac{1}{k_R}\sqrt{\frac{2\rho}{\pi f_{1,2}\mu_0\mu_r}}, \tag{3}$$

where $k_R \approx 1.4$ is the coefficient of reduction of penetration depth for a ferromagnetic medium; f_1, f_2 are the frequencies of induced currents in the full-scale and model rods; $\mu_0 = 4\pi\cdot10^{-7}$ H/m is the magnetic constant; μ_r is the relative value of the steel magnetic permeability. For nonferromagnetic steel, which lost its magnetic properties, when its temperature rose above the Curie point (approximately 740 °C), $k_R = 1$ and $\mu_r = 1$.

Having divided Δ_1 by Δ_2, using expressions (1)–(3), we will have:

$$m_l = \frac{\Delta_1}{\Delta_2} = \sqrt{\frac{f_2}{f_1}} = \frac{1}{\sqrt{m_f}}, \tag{4}$$

where m_f is he scale of current frequency.

$$m_l = \frac{f_1}{f_2} = \frac{1}{m_l^2}, \tag{5}$$

Time is inversely proportional to frequency $t \sim 1/f$. Thus, the time scale per one period of current oscillation m_t, allowing for expression (5), will be equal to:

$$m_t = \frac{t_1}{t_2} \sim \frac{f_2}{f_1} = \frac{1}{m_f} = m_l^2. \tag{6}$$

In keeping with the law of electromagnetic induction, the voltage in the full-scale and model cylindrical rods (in the first approximation) is:

$$U_{1,2} = 2\pi f_{1,2} B_{1,2} S_{1,2}, \tag{7}$$

where S_1, S_2 are the cross-sectional areas through which the magnetic flux passes in the rods. At high frequencies

$$S_{1,2} = \pi k_d d_{1,2} \Delta_{1,2}, \tag{8}$$

where k_d is the coefficient of reduction of the rod diameter, approximately by the depth of the magnetic flux penetration. This coefficient is the same for both the rods.

The voltage scale m_U, allowing for expressions (1), (2), (5), (7) and (8), is equal to:

$$m_U = \frac{U_1}{U_2} \approx \frac{f_1 d_1 \Delta_1}{f_2 d_2 \Delta_2} = m_f m_l m_l, \tag{9}$$

that corresponds to m_B scale.

Electric resistance of rod regions, through which the current flows is:

$$R_{1,2} = \rho\pi k_d \frac{d_{1,2}}{S'_{1,2}}, \tag{10}$$

where S_1, S_2 are the cross-sectional areas, through which current passes in the rods. At high frequencies:

$$S'_1 \approx \Delta_{1,2} l_{1,2}. \tag{11}$$

Scale of electric resistance m_R, allowing for expressions (2), (10) and (11), is equal to:

$$m_R = \frac{R_1}{R_2} \approx \frac{d_1 \Delta_2 l_2}{d_2 \Delta_1 l_1} = \frac{m_l}{m_l m_l} = \frac{1}{m_l}. \tag{12}$$

In keeping with Ohm's law the current is:

$$I_{1,2} = \frac{U_{1,2}}{R_{1,2}}. \tag{13}$$

Current scale m_1, taking into account expressions (9), (12) and (13), is equal to:

$$m_I = \frac{I_1}{I_2} = \frac{m_U}{m_R} = m_l. \tag{14}$$

Current density is:

$$J_{1,2} = \frac{I_{1,2}}{S'_{1,2}}. \quad (15)$$

Scale of current density m_J, taking into account expressions (2), (11), (14) and (15) is equal to:

$$m_J = \frac{J_1}{J_2} \approx \frac{I_1 \Delta_2 l_2}{I_2 \Delta_1 l_1} = \frac{m_I}{m_l m_l} = \frac{1}{m_l}. \quad (16)$$

Full and active power is:

$$S_{1,2} = U_{1,2} I_{1,2}; \quad P_{1,2} = I^2_{1,2} R_{1,2}. \quad (17)$$

The scales of full m_S and active power m_P taking into account expressions (9), (12), (14) and (17), are equal to:

$$m_s = \frac{S_1}{S_2} = m_U m_I = m_l; \quad m_P = \frac{P_1}{P_2} = m^2_I m_R = \frac{m^2_U}{m_R} = m_l. \quad (18)$$

Energy per one period of current oscillation is proportional to power and time $W \sim Pt$, its scale being m_w:

$$m_W = \frac{W_1}{W_2} \sim \frac{P_1 t_1}{P_2 t_2} = m_P m_t = m^3_l. \quad (19)$$

Flux linkage Ψ is:

$$\Psi_{1,2} = w\Phi_{1,2} = wB_{1,2} S_{1,2}, \quad (20)$$

where w is the number of turns, for rods $w = 1$; Φ_1, Φ_2 are the magnetic fluxes in the rods. Here, the scale of flux linkage m_Ψ and of magnetic fluxes m_Φ from expressions (1), (8) and (20) is as follows:

$$m_\Psi = \frac{\Psi_1}{\Psi_2} = \frac{d_1 \Delta_1}{d_2 \Delta_2} = m_l m_l = m^2_l; \; L_{1,2} = \frac{\Psi_{1,2}}{I_{1,2}}. \quad (21)$$

Inductance is:

$$L_{1,2} = \frac{\Psi_{1,2}}{I_{1,2}}. \quad (22)$$

Scale of inductance m_L taking into account expressions (1), (14), (20) and (22), is equal to:

$$m_L = \frac{L_1}{L_2} = \frac{\Psi_1 I_2}{\Psi_2 I_1} = \frac{m_\Psi}{m_I} = m_l. \quad (23)$$

Inductive (reactive) resistance is:

$$X_{1,2} = 2\pi f_{1,2} L_{1,2}. \quad (24)$$

Scale of inductive resistance m_x, taking into account expressions (5), (23) and (24), is equal to:

$$m_X = \frac{X_1}{X_2} = \frac{f_1 L_1}{f_2 L_2} = m_f m_I = \frac{1}{m_l}. \quad (25)$$

Scale of full resistance m_z, allowing for expressions (23) and (25) is:

$$m_Z = \frac{Z_1}{Z_2} = \sqrt{m^2_R + m^2_X} = \frac{1}{m_l}. \quad (26)$$

Similarity of thermal processes. Fourier criterion [16] for nonstationary thermal processes has the following form:

$$Fo = \frac{at'}{l^2}, \quad (27)$$

where a is the heat conductivity coefficient:

$$a = \frac{\lambda'}{\gamma c}, \quad (28)$$

where λ is the heat conductivity; γ is the density; c is the heat content (a, λ, γ and c are the same for the full-scale and model rods); t' is the heating (or cooling) time.

$$m'_t = \frac{t'_1}{t'_1} = \left(\frac{l_1}{l_2} \right) = m^2_l. \quad (29)$$

The rate of heating v of the rod sections is directly proportional to temperature T and is inversely proportional to time t', $v \sim T/t'$. As the temperatures should be the same, the scale of the rate for thermal processes of the rod heating m_v, is as follows, allowing for expression (29):

$$m_v = \frac{v_1}{v_2} \sim \frac{t'_2}{t'_1} = \frac{1}{m_{t'}} = \frac{1}{m^2_l}. \quad (30)$$

Model scaling. For a full-scale sample the current frequency of the thyristor frequency converter is f_1 = = 2.4 kHz, for a model sample the thyristor frequency converter has current frequency f_2 = 130 kHz. The scale coefficient of frequency by formula (5) is m_f = = $18.462 \cdot 10^{-3}$, while the scale coefficient of linear dimensions by formula (4) is m_l = 7.36.

The depths of penetration of induced currents in the full-scale and model rods by formula (3) (at $\rho_{850\ °C} \approx 7.76 \cdot 10^{-7}$ Ohm·m) are Δ_1 = 9.05 mm, Δ_2 = = 1.23 mm in the case, when the steel has lost its magnetic properties.

The full-scale sample diameter is d_1 = 62.7 mm. We will use the scale factor of linear dimensions to determine the model sample diameter $d_2 = d_1/m_1 \approx 8.5$ mm.

In Table 1 we will give the values of scale factor for the model rod, and in Table 2 — the initial data for

Table 1. Values of induction system scale factors

Parameter	Transition factor	Scale factor
Linear dimensions l	$m_l = 1/\sqrt{m_f}$	7.360
Current frequency f	$m_f = 1/m_l^2$	$18.46 \cdot 10^{-3}$
Current period T	$m_t = m_l^2$	54.200
Current I	$m_I = m_l$	7.360
Electric resistance R	$m_R = 1/m_l$	0.135
Current density J	$m_J = 1/m_l$	0.135
Power S	$m_S = m_l$	7.360
Power P	$m_P = m_l$	7.360
Energy W	$m_W = m_l^3$	398.680
Flux linkage Ψ	$m_\Psi = m_l^2$	54.20
Inductance L	$m_L = m_l$	7.360
Reactance X	$m_X = 1/m_l$	7.360
Impedance Z	$m_Z = 1/m_l$	0.135

numerical modeling of this «inductor–rod» induction system.

The computational domain of the studied model of the induction system is shown in Figure 2. It contains a three-turn water-cooled inductor Ω_1, from a copper conductor in the form of a round tube with an internal rectangular concentrator of the magnetic field and is a source of variable magnetic field of specified frequency. The product being heated is a sample in the form of a solid cylindrical rod Ω_2 from high-carbon ferromagnetic rail steel with simulation of the welded joint HAZ Ω_3 in its center and of ambient air Ω_4. From the viewpoint of axial symmetry, the mathematical model is represented in a two-dimensional cylindrical axisymmetric system of coordinates $r0z$. The electromagnetic problem was considered in the frequency domain, and the thermal nonstationary problem — in the time domain. The following physical processes were taken into account at modeling: joulean heating of sample metal due to eddy currents generated in it, thermal conductivity in the metal volume, heat losses for radiation and convection.

The process of induction heating is described by a nonlinear interdependent system of Maxwell and

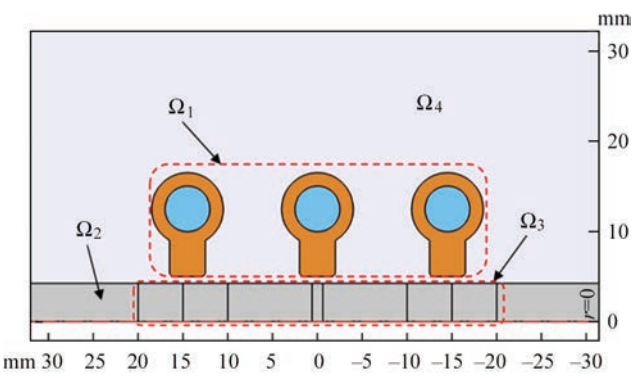

Figure 2. Axisymmetric model of the induction system

Table 2. Initial data for numerical modeling of «inductor–rod» system

Parameter	High-carbon steel (0.8 % C)
Sample length, mm	110
Sample diameter, mm	8.5
Ambient temperature, °C	20
Initial sample temperature, °C	20
Supply current frequency, kHz	130
Inductor current, A	200
Specified temperature of zone heating, °C	850…900
Outer diameter of the inductor, mm	28–33*
Inner diameter of the inductor, mm	8.75–10.75*
Inductor width, mm	28–38*
Distance between inductor windings, mm	7–10*
Tube diameter, mm	6
*Initial values for parametric investigation of the inductor geometrical dimensions.	

Fourier equations for the electromagnetic and thermal fields with the respective boundary conditions [16].

In order to solve the electromagnetic part of the calculation, the system of Maxwell equations is presented in the differential form:

$$\text{rot}\bar{H} = \bar{J} + \frac{\partial \bar{D}}{\partial t}; \quad \text{rot}\bar{E} = -\frac{\partial \bar{B}}{\partial t}; \quad \text{div}\bar{D} = \rho_e; \quad \text{div}\bar{B} = 0, \tag{31}$$

where $\bar{H}$, $\bar{E}$ are the vectors of magnetic and electric field intensities; $\bar{D}$, $\bar{B}$ are the vectors of electric and magnetic induction; $\bar{J}$ is the vector of conduction current density; $\bar{J} = \sigma\bar{E}$; σ is the specific electric conductivity; ρ_e is the density of extraneous electric charge.

Density of bias current $\frac{\partial \bar{D}}{\partial t}$ does not have any noticeable influence up to megahertz frequency range, as the conduction current density is much higher than that of bias current, so that it can be ignored, and then the equation becomes:

$$\text{rot}\bar{H} = \bar{J}. \tag{32}$$

The system of equations (31) was complemented by material equations for establishing a connection between the magnetic field intensity and magnetic induction, electric bias and electric field intensity, characterizing the electric and magnetic properties of the environment:

$$\bar{B} = \mu_0 \mu_r \bar{H}; \quad \bar{D} = \varepsilon_0 \varepsilon_r \bar{E}, \tag{33}$$

where ε_0 is the absolute dielectric permeability of the material; ε_r is the relative dielectric permeability of the material.

Numerical calculation of the electromagnetic fields of the induction system by finite element method is performed, using the representation of the distribution of vectors $\bar{H}$, $\bar{E}$ in the form of potential functions, and the equations are written using the vector magnetic potential $\bar{A}$ and scalar electric potential $\bar{V}$ which are defined as follows:

$$\bar{B} = \text{rot}\bar{A}; \quad \bar{E} = -\frac{\partial \bar{A}}{\partial t} - \text{grad}\bar{V}. \tag{34}$$

As in the axisymmetric model the currents are directed normal to the geometrical model plane, the vector magnetic potential $\bar{A}_\varphi$ has a single component (0, φ, 0), unlike $\bar{H}$, $\bar{B}$ fields, which have two components (*r*, *z*) in this plane.

Proceeding from the system of Maxwell equations, and allowing for the assumptions made and the connections for the conducting sections (of the inductor and steel rod) the differential equations will be written in the following form:

$$\nabla\left(\frac{\nabla}{\mu_0 \bar{A}}\right) = \bar{J}_0;$$
$$j\omega\sigma(T)\bar{A} + \nabla \times \left(\frac{\nabla}{\left(\mu_0 \mu_r(T)\right)} \bar{A}\right) = 0, \tag{35}$$

where ∇ is the nabla operator; $\bar{J}_0$ is the vector of current density; $j = \sqrt{-1}$ is the imaginary unit; ω is the angle frequency of the field, $\omega = 2\pi f$. Here, σ and μ_r depend on temperature *T*.

For correct calculation of the induction system parameters, it is necessary to take into account the dependence of electrophysical properties of steel on temperature *T*, as well as the loss of magnetic properties by it after reaching the temperature of the Curie point — T_k that will change the depth of penetration of the magnetic field and eddy currents into steel, resonance frequency and quality factor of the induction system.

In order to determine the magnetic permeability μ of the steel sample with carbon content in the range of 0.5–1.0 %, depending on magnetic field intensity $\bar{H}_0$ and temperature, an approximation function of the following form was adopted [18]:

$$\mu\left(H_0, T\right) = \begin{cases} 1 + \dfrac{\alpha' H_0^{\beta'} - 1}{\left[1 + \left(\dfrac{T}{T_K - T}\right)^{\chi'}\right]^{\delta'}}, \text{ if } T < T_K; \\ 1, \text{ if } T \geq T_K, \end{cases} \tag{36}$$

where $\alpha' = 3 \cdot 10^5$; $\beta' = -0.85$; $\chi' = 1.9$; $\delta' = 0.16$ are the approximation factors.

At modeling of the process of induction heating, the following was assigned as the boundary conditions of the electromagnetic part of the problem: on axis of symmetry 0*z* the Neumann condition $\frac{\partial \bar{H}}{\partial t} = 0$ — absence of the tangential component of the magnetic field intensity; Dirichlet condition $\bar{A}_\varphi = 0$ — presence of magnetic insulation on the outer boundaries, when the field is localized within the calculated region. The condition of constant temperature (30 °C) in the inductor turns due to cooling was accepted in a similar way.

In order to solve the nonstationary thermal problem in the time domain [16], Fourier equation, describing the temperature field distribution, was used:

$$\gamma c(T)\frac{\partial T}{\partial t} - \nabla\lambda\nabla T = Q, \tag{37}$$

where *Q* is the specific power of the heat sources.

Considering the nonlinear nature of the dependencies of physical parameters γ, *c*, λ, and σ on temperature *T*, in equation (37) they were assigned by the interpolation functions based on reference data for the high-carbon steel.

Calculation of specific power of inner heat sources links the electromagnetic problem to the thermal problem through determination of ohmic losses from the induced eddy currents in the sample that has a non-zero resistance, and non-zero density, according to Joule–Lentz law:

$$P = \frac{1}{n}\sum_{i=1}^{n}\frac{\bar{J}_i}{\sigma}, \tag{38}$$

where *P* is the evolving volumetric power; $\bar{J}_i$ is the total current density in integration point *i*.

In order to take into account thermal losses from convection and radiation from the side and end faces of the rod, the following expression was given:

$$q = -\bar{n}(-k\nabla T) = k(T - T_0) + \varepsilon\delta(T^4 - T_0^4). \tag{39}$$

where $\bar{n}$ is the unit outward normal vector; *k* is the convective heat transfer coefficient; T_0 is the ambient

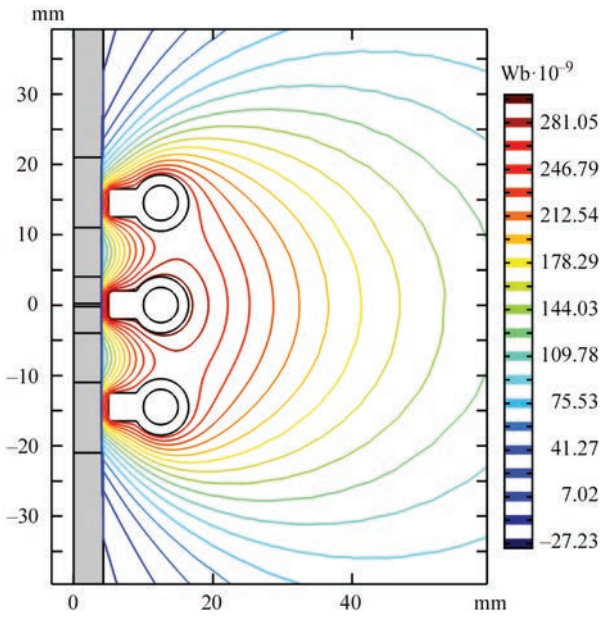

Figure 3. Distribution of force lines of the magnetic field of induction system

temperature; ε is the Stephan–Boltzmann constant; δ is the emissivity.

For correct accounting for the surface effect in the conductors and product, the computational grid cells were taken to be rectangular and very fine in the thin layer along the depth of magnetic field and eddy current penetration. In other areas the grid cells have the form of triangles.

Results of studying mathematical modeling of an induction system of heat treatment process. A distribution of the electromagnetic field of an induction system was derived as a result of solving the problem in the frequency domain (Figure 3). Due to the ring effect the lines of force of the magnetic field gather near the inductor inner surface and the rod outer surface with a high intensity of the magnetic field. Similarly, the current is concentrated in this area on the inner surface of the inductor conductors, namely on the edges of the rectangular concentrators of the magnetic field near the rod, and in the rod — on the surface under the inductor.

Figure 4, *a* shows the distribution of magnetic induction, $\bar{B}$, and Figure 4, *b* — distribution of current density, $\bar{J}$. The presented figures clearly show the ring effect and skin-effect in the inductor and rod conductors.

Figure 5, *a* shows the distribution of current density in the rod cross-section from its center to the side surface in its magnetic and non-magnetic state (temperature above the Curie point). On the rod surface in the magnetic state the current density is maximum and reaches the value of 422 A/mm^2. Closer to the rod center the current density drops abruptly and at the depth of 0.02 mm its value is equal to 313 A/mm^2; at the depth of 0.04 mm it is 234 A/mm^2; at the depth of 0.1 mm — 96 A/mm^2, and at the depth of 0.4 mm — just 2 A/mm^2. In the nonmagnetic state the current density is the highest on the rod surface and equal to 49 A/mm^2, at 4 mm distance from the rod center it is 30 A/mm^2, at 3 mm distance — 8 A/mm^2, and at 2 mm distance — 1 A/mm^2. Current density distribution in the axial direction on the rod surface is shown in Figure 5, *b*. Its peak values are determined under the rectangular concentrators of the magnetic field of inductor turns, where the distance to the rod surface is the shortest.

During modeling the energy parameters of the induction system were studied, depending on inductor current frequency f = 0.05–130.0 kHz. Figure 6, *a* shows the calculated dependencies of the total S_1, reactive Q_1 and active $P_1 = I^2 \cdot R$ power of the inductor, active power in a model rod $P_2 = Q$ and power factor $\cos\varphi = P_1/S_1$ (Figure 6, *b*). The active power release is enhanced with increase of current frequency that is

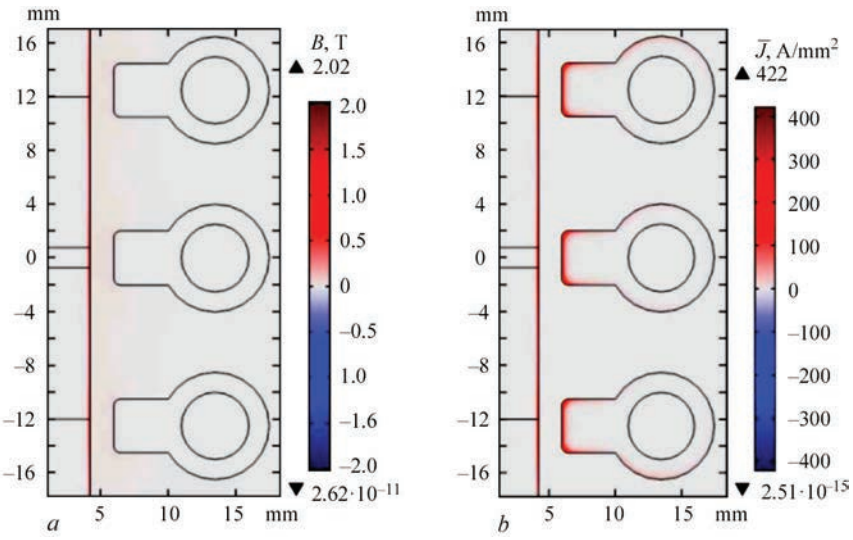

Figure 4. Distribution of induction system energy characteristics: *a* — magnetic induction; *b* — current density

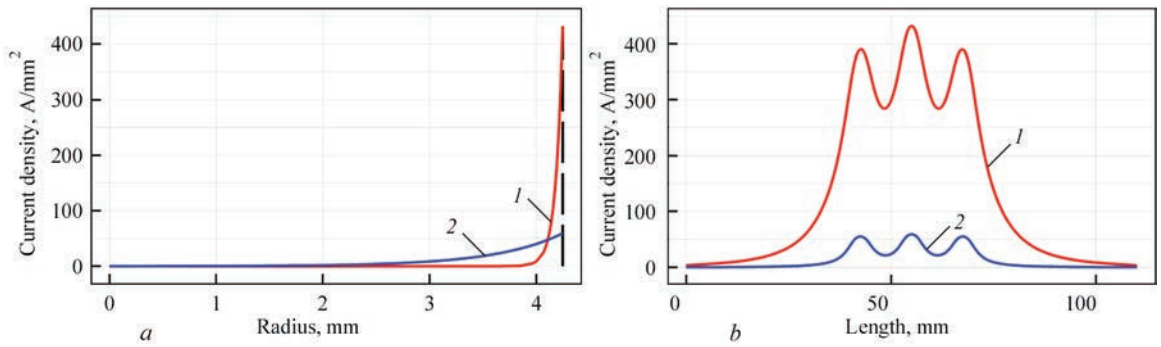

Figure 5. Distribution of current density in a model sample: *a* — in the rod cross-section from its center to the surface in its magnetic (*1*) and nonmagnetic (*2*) state; *b* — in the axial direction on the rod surface

related to reduction of the skin layer and increase of active resistance in the current passage path.

At calculation of the processes in the time domain the electromagnetic and thermal calculations were conducted sequentially, with refining of temperature-dependent parameters at each iteration step. In the electromagnetic part of the calculation, the most important parameter, which is transferred to the thermal part of the calculation, is the electric power, which evolves in the product and is responsible for heating. The ultimate goal of the calculation is obtaining a favorable distribution of the temperature field in the product at heat treatment of the sample with minimizing the thermal impact on the base metal beyond the welded joint. The welded joint proper consists of several different zones: fusion line (white band), zones of the coarse and fine grain, and softening zone. The metal in these zones has different structural components and different mechanical characteristics, which differ from the zone of base metal, which is not exposed to the thermal impact of welding. During modeling of heat treatment of metal in the welded joint zone, its heating was performed up to temperature somewhat higher than the structural transformation point A_{c3}, close to 850–900 °C, at which the required structural transformations of metal in the welded joint zone take place, to ensure a uniform structure of the metal.

During parametric solution of the problem, in order to obtain the required temperature field, the geometrical design parameters of the inductor — its width of 33 mm, interaxial distance of 8 mm, inner diameter of 9.75 mm and outer diameter of 30 mm were determined.

Figure 7 shows the distribution of the induction system temperature field at the end of the heating cycle. These geometrical parameters of the inductor provide the required temperature field and heating temperature above that of the start of phase transformations in the area of the sample welded joint that will allow achieving the required structural transformations in the joint metal.

Figure 8, *b* shows the location of points for temperature monitoring, when solving the thermal problem in different zones of the welded joint and the rod base metal zone.

In Figure 9 the graphs of temperature variation with time in these points were plotted. One can see that the process of sample heating can be divided into two characteristic regions. The first is the region of heating the ferromagnetic metal to magnetic transformation point (Curie point), where the most intensive

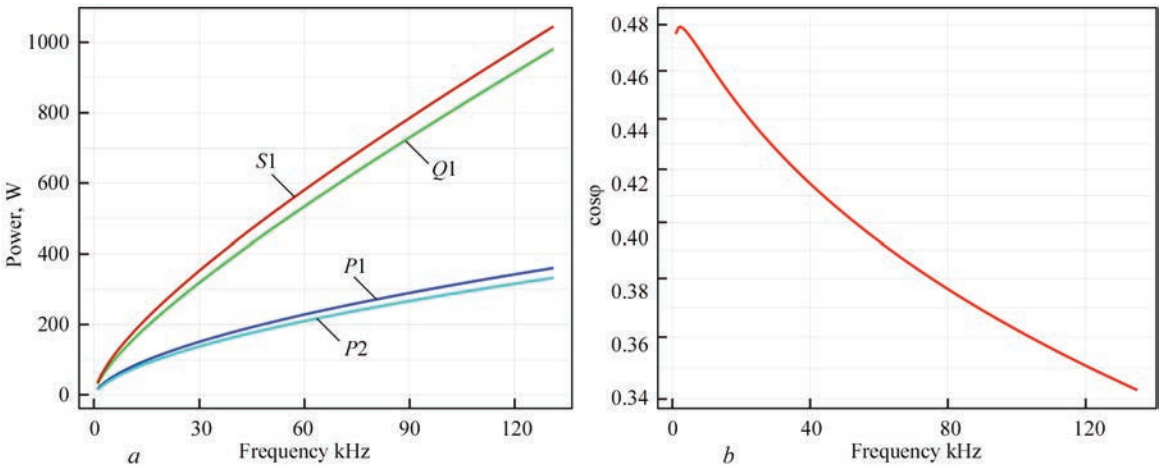

Figure 6. Energy parameters of induction system, depending on inductor current frequency: *a* — S_1, Q, P_1 and P_2; *b* — power factor cosφ

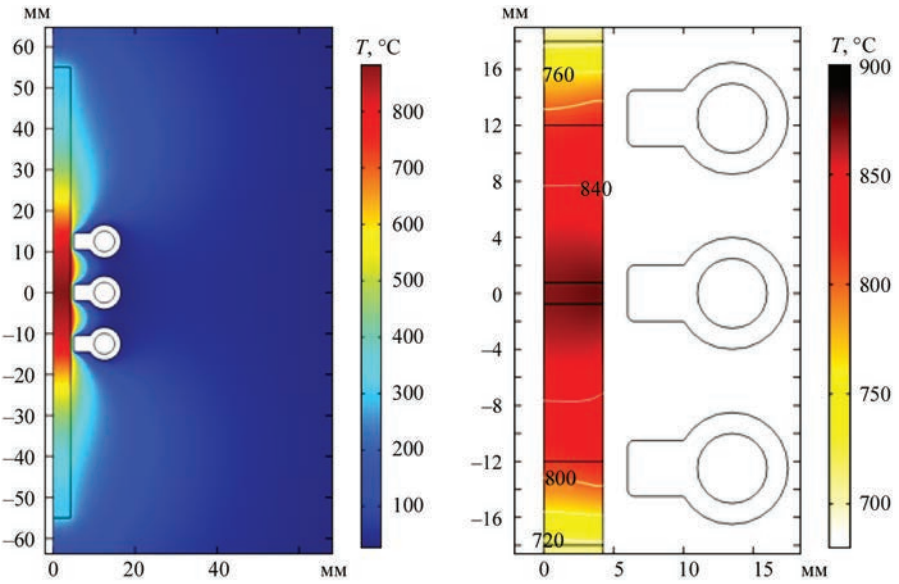

Figure 7. Temperature field distribution in the sample longitudinal section

heating takes place due to absorption of the electromagnetic energy by a thin skin-layer and high density of induced current flowing in it, with considerable evolution of thermal power and temperature propagation to the deep layers due to heat conductivity. In the second region a lowering of heating intensity is observed, because of the metal loosing its magnetic properties and of an increase in the depth of current penetration at lowering of its density with reduction of the released thermal power and lowering of heating intensity.

Physical modeling of the process of induction heat treatment of a model sample. The parameters determined from earlier performed mathematical modeling were used to conduct experiments on physical modeling of the process of induction HT. Physical modeling was performed on a sample of 8.5 mm diameter and 110 mm length, which was cut out of the railway rail head from high-strength rail steel K76F with a welded joint, located in the sample center (Figure 8, *a*).

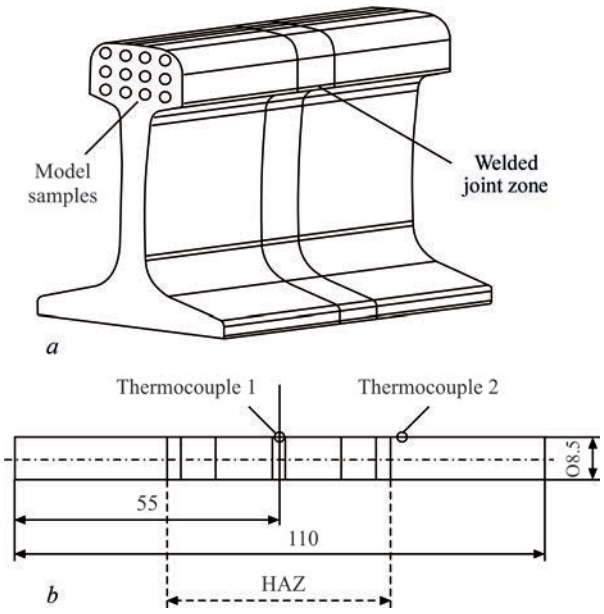

Figure 8. Sample for physical modeling of induction HT: *a* — illustration of the scheme of cutting out model samples from a welded joint of railway rail: *b* — layout of points for model sample temperature monitoring

Induction heating of the model sample was conducted using the developed low-power laboratory mock-up of a high-frequency power source based on a bridge inverter. The resonant oscillating circuit of the laboratory mock-up operates by the series type of RLC-circuit connection, where the model sample is the load. The copper three-turn water-cooled inductor with a magnetic field concentrator is placed above the welded joint zone. A battery of compensation capacitors and a matching transformer are connected. The power of the laboratory mock-up of the high-frequency current source for induction HT is equal to 2 kW, current frequency is 130 kHz. Rogowsky belt and digital oscilloscope Siglent SDS 1102CLM+ were used to control the inductor current, frequency, shape and amplitude of inductor voltage. To monitor the temperature change in the model sample, two reference points were defined: the first was thermocouple 1 (Figure 8) in the sample central part on its surface, to determine the maximum temperature of sample heating, and the second was thermocouple 2 at the end of welded joint HAZ to monitor the temperature field propagation in keeping with mathematical modeling. Used as sensors for temperature monitoring, were chromel-alumel thermocouples of K type of 0.75 mm diameter, which were welded-on in the specified points on the sample surface by capacitor-discharge welding. Conversion of the signal from thermocouple sensors in real time was performed by ADC L-Card E20-10

and galvanic decoupling block Promsad PSA0101, as well as special software for computer visualization of the derived data.

The thermal cycle of the induction heating process was determined, when conducting the experiments on physical modeling of induction HT of an experimental model sample from high-strength rail steel (Figure 9). At physical modeling the sample maximum temperature in the first reference point was equal to 882 °C for 180 s of the heating process, and in the second reference point it was 578 °C for 180 s. When comparing the calculated and experimental thermal cycles the largest error was close to 10 %. The calculation data obtained with application of the finite element method and measurement data at physical modeling of the thermal cycles lead to the conclusion that the calculated temperature change in the mathematical model agrees well with the experimental data. This allows using it for the next modeling step: determination of structural transformations in the welded joint metal under the impact of technological parameters of heat treatment that enables optimizing the technological processes of induction heat treatment of welded butt joints of railway rails.

Results of investigations at induction system modeling. Analysis of the presented results shows the correct solution of the problem, allowing for the physical processes and phenomena during modeling of the induction heating process. The developed mathematical model for numerical modeling of the process of high-frequency induction heating of a model sample of welded joint on high-carbon, high-strength rail steel, derived on the base of the similarity theory, allows establishing the parameters and configuration of «inductor–product» system for performance of induction HT of a sample, and determination of the space-time distribution of the temperature field during performance of its HT. Then the results of the first part of the modeling problem should be transferred to the second part, where modeling of the kinetics of phase transformations and weld metal properties will be performed, depending on the process thermal cycle, which will allow determination of the range of optimally required parameters of HT process. After numerical calculation, the obtained data will be used during physical modeling, with optimization of the modes of sample HT, and it will help significantly reduce the number of the conducted experiments on determination of the thermal cycle impact on the features of phase transformation kinetics and mechanical properties in the welded joint zone. At achievement of satisfactory results on a model sample, it is necessary to go over to investigation of the process of induction heating at HT of the metal of weld and near-weld zone

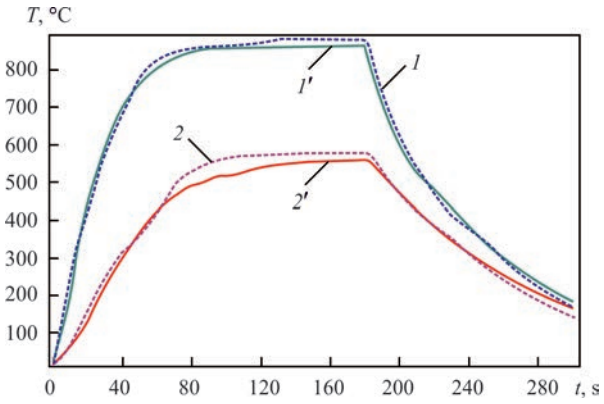

Figure 9. Change of temperatures in time in reference points of the model sample: *1*, *2* — thermal cycle during physical modeling; *1′*, *2′* — calculated data from mathematical modeling

of a real product — the rail, while performing recalculation of the parameters by the similarity theory, following the established HT modes and refining them, as well as correcting the inductor configuration.

Conclusions

1. To simplify physical modeling of induction heating, the theory of similarity of the electromagnetic processes was used to reduce the overall dimensions of a model cylindrical rod using the scale factors.

2. The developed mathematical model for numerical modeling of the process of high-frequency induction heating of a welded joint sample from high-carbon high-strength rail steel allows determination of optimum geometrical and energy parameters of «inductor–product» system.

3. The numerical solution of an axisymmetric problem, taking into account the main nonlinear dependencies of the induction model, allows modeling the space-time distribution of the temperature field.

4. Proceeding from determination of the main energy parameters of «inductor–product» system, a parametric search for optimum geometrical parameters of the inductor was performed, and the required distribution of the temperature field in the zone of the sample welded joint was obtained.

5. When modeling of thermal heating of a welded joint sample was performed, the temperature field of the sample with the weld was determined that allows modeling the change of the space-time structural-phase state of the metal during heat treatment.

6. The proposed mathematical and physical models of model sample heating can be used, when solving the problem of optimization of induction heat treatment of welded joints of railway rails. Use of these data at determination of key parameters of the heat treatment process on model samples allows going over to heat treatment of welded joints of the real

railway rails in the welded joint zone, based on the similarity theory.

1. Gubatyuk, R.S. (2019) Heat treatment of welded joints of high-strength railway rails (Review). *The Paton Welding J.*, **2**, 41–48. doi: https://doi.org/10.15407/tpwj2019.02.07
2. Kuchuk-Yatsenko, S.I., Antipin, E.V., Didkovskyi, O.V. et al. (2020) Evaluation of quality of welded joints of high-strength railway rails of modern production taking into account the requirements of Ukrainian and European standards. *Ibid.*, **7**, 3–11. DOI: https://doi.org/10.37434/tpwj2020.07.01
3. Rezanov, V.A., Fedin, V.M., Bashlykov, A.V. (2013) Differentiated hardening of rail welded joints. *Vestnik VNIIZhT*, **2**, 28–34 [in Russian].
4. Dolgikh, I.Yu., Korolyov, A.N., Zakharov, V.M. (2014) Simulation of thermal processes dynamics under induction heating. *Vestnik ISEU*, **5**, 1–7 [in Russian].
5. Pleshivtseva, Yu. E., Popov, A. V., Popova, M. A., Derevyanov, M. Yu. (2019) Optimal inductor design for surface hardening of cylindrical billets based on numerical two-dimensional model. Vestnik of Astrakhan State Technical University. Series: Management, *Computer Science and Informatics*, **1**, 40–50. DOI: https://doi.org/10.24143/2072-9502-2019-1-40-50
6. Chao, Yu, Hong, Xiao, Zi-chen, Qi, Yun-peng, Zhao (2019) Finite element analysis and experiment on induction heating process of slab continuous casting-direct rolling. *Metallurgical Research & Technology*, 116 (**4**), 403. doi: https://doi.org/10.1051/metal/2018117
7. Li, F., Ning, J., Liang, S. (2019) Analytical modeling of the temperature using uniform moving heat source in planar induction heating process. *Applied Sci.*, **9**, 14–45. DOI: https://doi.org/10.3390/app9071445
8. Takeuchi, H., Yogo, Y. (2019) An induction heating analysis with consideration of temperature dependent B-H curves and change in phase transformation under rapid heating. *ISIJ Int.*, **59**, 551–558. DOI: https://doi:10.2355/isijinternational.isijint-2018-552
9. Javaheri, V., Asperheim, J.I., Grande, B. et al. (2020) Simulation and experimental studies of induction hardening behavior of a new medium-carbon, low-alloy wear resistance steel. *COMPEL — the International J. for Computation and Mathematics in Electrical and Electronic engineering*, 39(**1**), 158–165. DOI: https://doi.org/10.1108/COMPEL-06-2019-0227
10. Gubatyuk, R.S., Rymar, S.V., Prokofiev, O.S. et al. (2021) Simulation of electromagnetic and thermal fields in the process of induction heating on small specimens with the presence of welded joint of high-strength railway rails. *The Paton Welding J.*, **1**, 44–49. DOI: https://doi.org/10.37434/as2021.01.08
11. Roppert, K., Toth, F., Kaltenbacher, M. (2020) Modeling nonlinear steady-state induction heating processes. *IEEE Transact. on Magnetics*, 56 (**3**). DOI: https://doi.org/10.1109/tmag.2019.2957343
12. Venikov, V.A. (1966) *Similarity theory and modeling as applied to the problems of the electric power industry*. Moscow, Vysshaya Shkola [in Russian].
13. Paton, B.E., Lebedev, V.K. (1969) *Electrical equipment for resistance welding.* Moscow, Mashinostroenie [in Russian].
14. Pentegov, I.V., Rymar, S.V., Levin, M.I., Lavrenyuk, A.V. (2015) Determination of magnetic inductions in the magnetic circuits of power transformers with the combined use of anisotropic and isotropic electrical steels. *Elektrotekhnika i Elektromekhanika*, **6**, 31–35 [in Russian]. DOI: https://doi.org/10.20998/2074-272X.2015.6.05
15. Kutateladze, S.S. (1982) *Similarity analysis in thermal physics.* Novosibirsk, Nauka [in Russian].
16. Landau, L.D., Lifshits, E.M. (2006) *Field theory. Theoretical physics*. Moscow, Fizmatlit [in Russian].
17. Pentelyat, M.G., Shulzhenko, N.G. (2007) Use of vector magnetic potential in finite element analysis of non-stationary three-dimensional electromagnetic fields in conducting media. *Elektrotekhnika i Elektromekhanika*, **5**, 42–47 [in Russian].
18. Vladimirov, S.N., Zeman, S.K., Ruban, V.V. (2009) Analytical relations approximating the temperature-field dependence of the magnetic permeability of structural steels. *Izv. TPU*, 315(**4**), 100–104 [in Russian].

Received 12.07.2021